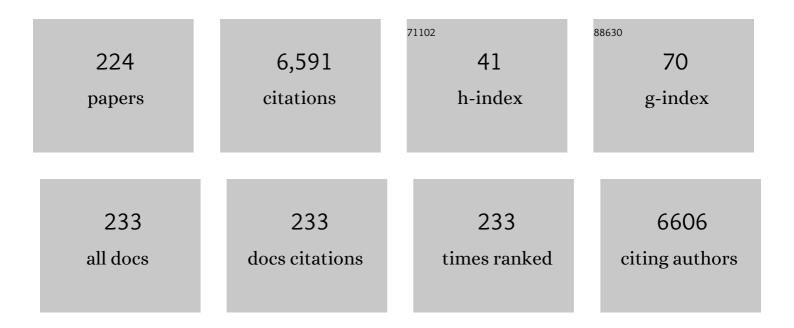
List of Publications by Year in descending order

Source: https://exaly.com/author-pdf/2400962/publications.pdf Version: 2024-02-01



#	Article	IF	CITATIONS
1	Nanodomain structure ofPb[Zr1â^'xTix]O3at its morphotropic phase boundary: Investigations from local to average structure. Physical Review B, 2007, 75, .	3.2	264
2	Host Materials Anchoring Polysulfides in Li–S Batteries Reviewed. Advanced Energy Materials, 2021, 11, 2001304.	19.5	254
3	Powerâ€ŧoâ€5yngas: An Enabling Technology for the Transition of the Energy System?. Angewandte Chemie - International Edition, 2017, 56, 5402-5411.	13.8	212
4	A Review of Degradation Mechanisms and Recent Achievements for Niâ€Rich Cathodeâ€Based Liâ€lon Batteries. Advanced Energy Materials, 2021, 11, 2103005.	19.5	206
5	Structural and dynamic properties of oxygen vacancies in perovskite oxides—analysis of defect chemistry by modern multi-frequency and pulsed EPR techniques. Physical Chemistry Chemical Physics, 2011, 13, 368-384.	2.8	202
6	Quantitative and time-resolved detection of lithium plating on graphite anodes in lithium ion batteries. Materials Today, 2018, 21, 231-240.	14.2	163
7	Strategies towards enabling lithium metal in batteries: interphases and electrodes. Energy and Environmental Science, 2021, 14, 5289-5314.	30.8	156
8	Singlet Oxygen Formation during the Charging Process of an Aprotic Lithium–Oxygen Battery. Angewandte Chemie - International Edition, 2016, 55, 6892-6895.	13.8	146
9	Operando electron paramagnetic resonance spectroscopy – formation of mossy lithium on lithium an anodes during charge–discharge cycling. Energy and Environmental Science, 2015, 8, 1358-1367.	30.8	128
10	Defect structure of oxide ferroelectrics—valence state, site of incorporation, mechanisms of charge compensation and internal bias fields. Journal of Electroceramics, 2007, 19, 11-23.	2.0	120
11	Defect-Dipole Formation in Copper-Doped <mml:math xmlns:mml="http://www.w3.org/1998/Math/MathML" display="inline"&gt;<mml:msub><mml:mi>PbTiO</mml:mi><mml:mn>3</mml:mn></mml:msub>Ferroe Physical Review Letters, 2008, 100, 095504.</mml:math 	electrics.	118
12	Synthesis, Characterization, Defect Chemistry, and FET Properties of Microwave-Derived Nanoscaled Zinc Oxide. Chemistry of Materials, 2010, 22, 2203-2212.	6.7	117
13	Reorientation of (MnTi″â^VO••)× defect dipoles in acceptor-modified BaTiO3 single crystals: An electron paramagnetic resonance study. Applied Physics Letters, 2008, 93, .	n 3.3	111
14	Association of oxygen vacancies with impurity metal ions in lead titanate. Physical Review B, 2007, 76, .	3.2	94
15	Singlet Oxygen Formation during the Charging Process of an Aprotic Lithium–Oxygen Battery. Angewandte Chemie, 2016, 128, 7006-7009.	2.0	87
16	Characterization of Defect Structure in Acceptor-Modified Piezoelectric Ceramics by Multifrequency and Multipulse Electron Paramagnetic Resonance Spectroscopy. Journal of the American Ceramic Society, 2008, 91, 691-701.	3.8	82
17	Insights into a layered hybrid solid electrolyte and its application in long lifespan high-voltage all-solid-state lithium batteries. Journal of Materials Chemistry A, 2019, 7, 3882-3894.	10.3	82
18	Defect structure and materials "hardening―in Fe2O3-doped [Bi0.5Na0.5]TiO3 ferroelectrics. Applied Physics Letters, 2010, 97	3.3	79

#	Article	IF	CITATIONS
19	Position of defects with respect to domain walls in Fe3+-doped Pb[Zr0.52Ti0.48]O3 piezoelectric ceramics. Applied Physics Letters, 2011, 98, .	3.3	77
20	Effect of Nb-donor and Fe-acceptor dopants in (Bi1/2Na1/2)TiO3–BaTiO3–(K0.5Na0.5)NbO3 lead-free piezoceramics. Journal of Applied Physics, 2010, 108, .	2.5	75
21	CuO as a sintering additive for (Bi1/2Na1/2)TiO3–BaTiO3–(K0.5Na0.5)NbO3 lead-free piezoceramics. Journal of the European Ceramic Society, 2011, 31, 2107-2117.	5.7	72
22	Processing of Manganese-Doped [Bi0.5Na0.5]TiO3 Ferroelectrics: Reduction and Oxidation Reactions During Calcination and Sintering. Journal of the American Ceramic Society, 2011, 94, 1363-1367.	3.8	70
23	Monolithic All-Phosphate Solid-State Lithium-Ion Battery with Improved Interfacial Compatibility. ACS Applied Materials & Interfaces, 2018, 10, 22264-22277.	8.0	68
24	Interface Aspects in Allâ€Solidâ€State Liâ€Based Batteries Reviewed. Advanced Energy Materials, 2021, 11, 2003939.	19.5	66
25	Axial Solvent Coordination in "Base-Off―Cob(II)alamin and Related Co(II)-Corrinates Revealed by 2D-EPR. Journal of the American Chemical Society, 2003, 125, 5915-5927.	13.7	62
26	Local variations in defect polarization and covalent bonding in ferroelectric Cu2+-doped PZT and KNN functional ceramics at the morphotropic phase boundary. Physical Chemistry Chemical Physics, 2009, 11, 8698.	2.8	62
27	Interactions of defect complexes and domain walls in CuO-doped ferroelectric (K,Na)NbO3. Applied Physics Letters, 2013, 102, .	3.3	62
28	Influence of microstructure and AlPO <sub>4</sub> secondary-phase on the ionic conductivity of Li1.3Al0.3Ti1.7(PO4)3 solid-state electrolyte. Functional Materials Letters, 2016, 09, 1650066.	1.2	61
29	Superionic bulk conductivity in Li1.3Al0.3Ti1.7(PO4)3 solid electrolyte. Solid State Ionics, 2017, 309, 180-186.	2.7	60
30	High-frequency electron paramagnetic resonance investigation of the Fe3+ impurity center in polycrystalline PbTiO3 in its ferroelectric phase. Journal of Applied Physics, 2004, 96, 7440-7444.	2.5	55
31	A Small Paramagnetic Platinum Cluster in an NaY Zeolite:Â Characterization and Hydrogen Adsorption and Desorption. Journal of Physical Chemistry B, 2006, 110, 2013-2023.	2.6	55
32	Improving the rate capability of high voltage lithium-ion battery cathode material LiNi0.5Mn1.5O4 by ruthenium doping. Journal of Power Sources, 2014, 267, 533-541.	7.8	55
33	Temperature-dependent cycling performance and ageing mechanisms of C6/LiNi1/3Mn1/3Co1/3O2 batteries. Journal of Power Sources, 2018, 396, 444-452.	7.8	55
34	Double-Shelled Co <sub>3</sub> O <sub>4</sub> /C Nanocages Enabling Polysulfides Adsorption for High-Performance Lithium–Sulfur Batteries. ACS Applied Energy Materials, 2019, 2, 8153-8162.	5.1	55
35	Iron-oxygen vacancy defect association in polycrystalline iron-modifiedPbZrO3antiferroelectrics: Multifrequency electron paramagnetic resonance and Newman superposition model analysis. Physical Review B, 2006, 73, .	3.2	48
36	Exploring the Interface of Skin‣ayered Titanium Fibers for Electrochemical Water Splitting. Advanced Energy Materials, 2021, 11, 2002926.	19.5	48

#	Article	IF	CITATIONS
37	Luminescence of heat-treated silicon-based polymers: promising materials for LED applications. Journal of Materials Science, 2008, 43, 5790-5796.	3.7	46
38	Silicon and Iron as Resource-Efficient Anode Materials for Ambient-Temperature Metal-Air Batteries: A Review. Materials, 2019, 12, 2134.	2.9	46
39	Self-standing NASICON-type electrodes with high mass loading for fast-cycling all-phosphate sodium-ion batteries. Journal of Materials Chemistry A, 2018, 6, 18304-18317.	10.3	44
40	Influence of sintering temperature on conductivity and mechanical behavior of the solid electrolyte LATP. Ceramics International, 2019, 45, 14697-14703.	4.8	43
41	Size effects in Fe3+-doped PbTiO3 nanocrystals—Formation and orientation of defect-dipoles. Journal of the European Ceramic Society, 2010, 30, 289-293.	5.7	42
42	RECENT DEVELOPMENTS AND FUTURE PERSPECTIVES OF LEAD-FREE FERROELECTRICS. Functional Materials Letters, 2010, 03, 1-4.	1.2	42
43	High-field/high-frequency EPR of paramagnetic functional centers in Cu2+- and Fe3+-modified polycrystalline Pb[ZrxTi1â^'x]O3 ferroelectrics. Magnetic Resonance in Chemistry, 2005, 43, S166-S173.	1.9	41
44	Formation of magnetic grains in ferroelectric Pb[Zr0.6Ti0.4]O3 ceramics doped with Fe3+ above the solubility limit. Applied Physics Letters, 2009, 94, 142901.	3.3	41
45	Degradation mechanisms of C6/LiNi0.5Mn0.3Co0.2O2 Li-ion batteries unraveled by non-destructive and post-mortem methods. Journal of Power Sources, 2019, 416, 163-174.	7.8	40
46	Tailored Gas Adsorption Properties of Electrospun Carbon Nanofibers for Gas Separation and Storage. ChemSusChem, 2020, 13, 3180-3191.	6.8	40
47	Insights into the reactive sintering and separated specific grain/grain boundary conductivities of [11.3AI0.3Ti1.7(PO4)3. Journal of Power Sources, 2021, 492, 229631 Manganese-doped <mmi:math <="" td="" xmins:mmi="http://www.w3.org/1998/Math/MathML"><td>7.8</td><td>40</td></mmi:math>	7.8	40
48	display="inline"> <mml:mrow> <mml:mo> (</mml:mo> <mml:mn> 1 </mml:mn> <mml:mo> â^ </mml:mo> <mml:mi> xmlns:mml="http://www.w3.org/1998/Math/MathML" display="inline"&gt; <mml:msub> <mml:mrow /&gt; <mml:mn> 3 </mml:mn> </mml:mrow </mml:msub>  †&lt;<mml:math xmlns:mml="http://www.w3.org/1998/Math/MathML"</mml:math </mml:mi></mml:mrow>	x3.2	> <mml:mo>) 39</mml:mo>
49	display="inline"> <mml:mi>x</mml:mi> PbTiO <mml:math ymlns:mml_"http://www.w3.org/199 Understanding the nanoscale redox-behavior of iron-anodes for rechargeable iron-air batteries. Nano Energy, 2017, 41, 706-716.</mml:math 	16.0	39
50	EPR Imaging of Metallic Lithium and its Application to Dendrite Localisation in Battery Separators. Scientific Reports, 2018, 8, 14331.	3.3	39
51	Characterization of (Fe <sub>Zr,Ti</sub> -V <sub>o</sub> <sup>ldrldr</sup> ) <sup>ldr</sup> defect dipoles in (La,Fe)-codoped PZT 52.5/47.5 piezoelectric ceramics by multifrequency electron paramagnetic resonance spectroscopy. IEEE Transactions on Ultrasonics, Ferroelectrics, and Frequency Control. 2008, 55, 1061-1068.	3.0	37
52	Defect structure and formation of defect complexes in Cu2+-modified metal oxides derived from a spin-Hamiltonian parameter analysis. Molecular Physics, 2009, 107, 1981-1986.	1.7	37
53	Defect structure in lithium-doped polymer-derived SiCN ceramics characterized by Raman and electron paramagnetic resonance spectroscopy. Physical Chemistry Chemical Physics, 2009, 11, 5628.	2.8	37
54	Synthesis of Ni-Rich Layered-Oxide Nanomaterials with Enhanced Li-Ion Diffusion Pathways as High-Rate Cathodes for Li-Ion Batteries. ACS Applied Energy Materials, 2020, 3, 6583-6590.	5.1	37

#	Article	IF	CITATIONS
55	Multifrequency electron paramagnetic resonance analysis of polycrystalline gadolinium-doped PbTiO3—Charge compensation and site of incorporation. Applied Physics Letters, 2006, 88, 122506.	3.3	36
56	Carbon-coated core–shell Li <sub>2</sub> S@C nanocomposites as high performance cathode materials for lithium–sulfur batteries. Journal of Materials Chemistry A, 2017, 5, 1428-1433.	10.3	36
57	Nanoâ€Scale Complexions Facilitate Li Dendriteâ€Free Operation in LATP Solidâ€State Electrolyte. Advanced Energy Materials, 2021, 11, 2100707.	19.5	36
58	Defect structure of the mixed ionic–electronic conducting Sr[Ti,Fe]Ox solid-solution system — Change in iron oxidation states and defect complexation. Solid State Ionics, 2011, 184, 47-51.	2.7	35
59	The carbonization of polyacrylonitrile-derived electrospun carbon nanofibers studied by <i>in situ</i> transmission electron microscopy. RSC Advances, 2019, 9, 6267-6277.	3.6	35
60	Molecular precursor derived and solution processed indium–zinc oxide as a semiconductor in a field-effect transistor device. Towards an improved understanding of semiconductor film composition. Journal of Materials Chemistry C, 2013, 1, 2577.	5.5	34
61	Development towards cell-to-cell monolithic integration of a thin-film solar cell and lithium-ion accumulator. Journal of Power Sources, 2016, 327, 340-344.	7.8	33
62	Overpotential analysis of graphite-based Li-ion batteries seen from a porous electrode modeling perspective. Journal of Power Sources, 2021, 509, 230345.	7.8	33
63	Defect structure in aliovalently-doped and isovalently-substituted PbTiO <sub>3</sub> nano-powders. Journal of Physics Condensed Matter, 2010, 22, 345901.	1.8	32
64	Cobalt substituted Pr2Ni1-Co O4+ (x = 0, 0.1, 0.2) oxygen electrodes: Impact on electrochemical performance and durability of solid oxide electrolysis cells. Journal of Power Sources, 2021, 482, 228909.	7.8	32
65	Direct Observation of SEI Formation and Lithiation in Thin-Film Silicon Electrodes via <i>in Situ</i> Electrochemical Atomic Force Microscopy. ACS Applied Energy Materials, 2019, 2, 6761-6767.	5.1	31
66	Local symmetry-reduction in tetragonal (La,Fe)-codoped Pb[Zr <sub>0.4</sub> Ti <sub>0.6</sub> ]O <sub>3</sub> piezoelectric ceramics. Physica Scripta, 2007, T129, 12-16.	2.5	30
67	FORMATION OF \$({m Ti}'_{m Ti} - V_{m O}^{ullet ullet})^{ullet}\$ DEFECT DIPOLES IN BaTiO3 CERAMICS HEAT-TREATED UNDER REDUCED OXYGEN PARTIAL-PRESSURE. Functional Materials Letters, 2010, 03, 65-68.	1.2	30
68	Long run discharge, performance and efficiency of primary Silicon–air cells with alkaline electrolyte. Electrochimica Acta, 2017, 225, 215-224.	5.2	30
69	Long-run <i>in operando</i> NMR to investigate the evolution and degradation of battery cells. Physical Chemistry Chemical Physics, 2018, 20, 13765-13776.	2.8	30
70	Modeling the degradation mechanisms of C6/LiFePO4 batteries. Journal of Power Sources, 2018, 375, 106-117.	7.8	30
71	Origin of Degradation in Siâ€Based Allâ€Solidâ€State Liâ€Ion Microbatteries. Advanced Energy Materials, 2018, 8, 1801430.	19.5	29
72	Efficient Area Matched Converter Aided Solar Charging of Lithium Ion Batteries Using High Voltage Perovskite Solar Cells. ACS Applied Energy Materials, 2020, 3, 431-439.	5.1	29

#	Article	IF	CITATIONS
73	Combined quantitative microscopy on the microstructure and phase evolution in Li1.3Al0.3Ti1.7(PO4)3 ceramics. Journal of Advanced Ceramics, 2020, 9, 149-161.	17.4	29
74	Determination of functional center local environment in copper-modified Pb[Zr0.54Ti0.46]O3 ceramics. Journal of Applied Physics, 2004, 95, 8092-8096.	2.5	28
75	New insight into the discharge mechanism of silicon–air batteries using electrochemical impedance spectroscopy. Physical Chemistry Chemical Physics, 2013, 15, 3256.	2.8	28
76	Microstructure of sodium-potassium niobate ceramics sintered under high alkaline vapor pressure atmosphere. Journal of the European Ceramic Society, 2014, 34, 4213-4221.	5.7	28
77	Quantitative Analysis of Time-Domain Supported Electrochemical Impedance Spectroscopy Data of Li-Ion Batteries: Reliable Activation Energy Determination at Low Frequencies. Journal of the Electrochemical Society, 2016, 163, H521-H527.	2.9	28
78	DEFECT STRUCTURE OF COPPER DOPED POTASSIUM NIOBATE CERAMICS. Functional Materials Letters, 2010, 03, 19-24.	1.2	26
79	Morphology Dependency of Li3V2(PO4)3/C Cathode Material Regarding to Rate Capability and Cycle Life in Lithium-ion Batteries. Electrochimica Acta, 2017, 232, 310-322.	5.2	26
80	Interaction and Reaction of Ethylene and Oxygen on Six-Atom Silver Clusters Supported on LTA Zeolite. Journal of Physical Chemistry C, 2009, 113, 19623-19632.	3.1	25
81	Limitation of Discharge Capacity and Mechanisms of Airâ€Electrode Deactivation in Silicon–Air Batteries. ChemSusChem, 2012, 5, 2278-2285.	6.8	25
82	Sol Gel vs Solid State Synthesis of the Fast Lithium-Ion Conducting Solid State Electrolyte Li <sub>7</sub> La <sub>3</sub> Zr <sub>2</sub> O <sub>12</sub> Substituted withÂlron. Journal of the Electrochemical Society, 2019, 166, A5403-A5409.	2.9	25
83	Double layer capacitances analysed with impedance spectroscopy and cyclic voltammetry: validity and limits of the constant phase element parameterization. Physical Chemistry Chemical Physics, 2021, 23, 21097-21105.	2.8	25
84	CuO-doped NaNbO <mml:math <br="" xmlns:mml="http://www.w3.org/1998/Math/MathML">display="inline"&gt;<mml:msub><mml:mrow /&gt;<mml:mn>3</mml:mn></mml:mrow </mml:msub></mml:math> antiferroelectrics: Impact of aliovalent doping and nonstoichiometry on the defect structure and formation of secondary phases. Physical Review B, 2011,	3.2	24
85	84, . Defect structure of non-stoichiometric and aliovalently doped perovskite oxides. Materials Technology, 2013, 28, 241-246.	3.0	24
86	High Power and High Capacity 3D-Structured TiO <sub>2</sub> Electrodes for Lithium-Ion Microbatteries. Journal of the Electrochemical Society, 2016, 163, A2385-A2389.	2.9	24
87	Powerâ€ŧo‣yngas – eine Schlüsseltechnologie für die Umstellung des Energiesystems?. Angewandte Chemie, 2017, 129, 5488-5498.	2.0	24
88	Monitoring local redox processes in LiNi0.5Mn1.5O4 battery cathode material by <i>in operando</i> EPR spectroscopy. Journal of Chemical Physics, 2018, 148, 014705.	3.0	23
89	Carbonisation temperature dependence of electrochemical activity of nitrogen-doped carbon fibres from electrospinning as air-cathodes for aqueous-alkaline metal–air batteries. RSC Advances, 2019, 9, 27231-27241.	3.6	23
90	In operando EPR investigation of redox mechanisms in LiCoO2. Chemical Physics Letters, 2019, 716, 231-236.	2.6	23

#	Article	IF	CITATIONS
91	All-ceramic Li batteries based on garnet structured Li <sub>7</sub> La <sub>3</sub> Zr <sub>2</sub> O <sub>12</sub> . Materials Technology, 2020, 35, 656-674.	3.0	22
92	Influence of Al Alloying on the Electrochemical Behavior of Zn Electrodes for Zn–Air Batteries With Neutral Sodium Chloride Electrolyte. Frontiers in Chemistry, 2019, 7, 800.	3.6	21
93	Reference electrode assembly and its use in the study of fluorohydrogenate ionic liquid silicon electrochemistry. Physical Chemistry Chemical Physics, 2013, 15, 17837.	2.8	19
94	LiTi <sub>2</sub> (PO <sub>4</sub> ) <sub>3</sub> /C Anode Material with a Spindleâ€Like Morphology for Batteries with High Rate Capability and Improved Cycle Life. ChemElectroChem, 2016, 3, 1157-1169.	3.4	19
95	Analysis of the effects of different carbon coating strategies on structure and electrochemical behavior of LiCoPO4 material as a high-voltage cathode electrode for lithium ion batteries. Electrochimica Acta, 2018, 279, 108-117.	5.2	19
96	Electrochemical and Electronic Charge Transport Properties of Ni-Doped LiMn2O4 Spinel Obtained from Polyol-Mediated Synthesis. Materials, 2018, 11, 806.	2.9	19
97	High-Temperature Co-Electrolysis: A Versatile Method to Sustainably Produce Tailored Syngas Compositions. Journal of the Electrochemical Society, 2019, 166, F971-F975.	2.9	19
98	Morphology-controllable synthesis of LiCoPO4 and its influence on electrochemical performance for high-voltage lithium ion batteries. Journal of Power Sources, 2020, 450, 227726.	7.8	19
99	Electron paramagnetic resonance studies of a platinum cluster in Linde L and faujasite zeolites. Physical Chemistry Chemical Physics, 2003, 5, 3076.	2.8	18
100	Local coordination of Fe3+ in Li[Co0.98Fe0.02]O2 as cathode material for lithium ion batteries—multi-frequency EPR and Monte-Carlo Newman-superposition model analysis. Physical Chemistry Chemical Physics, 2011, 13, 9344.	2.8	18
101	Processing of Al-doped ZnO protective thin films on aluminum current collectors for lithium ion batteries. Thin Solid Films, 2016, 619, 302-307.	1.8	18
102	Influence of Dopant Type and Orientation of Silicon Anodes on Performance, Efficiency and Corrosion of Silicon–Air Cells with EMIm(HF) <sub>2.3</sub> F Electrolyte. Journal of the Electrochemical Society, 2017, 164, A2310-A2320.	2.9	18
103	Performance and Degradation of Electrolyte-Supported Single Cell Composed of Mo-Au-Ni/GDC Fuel Electrode and LSCF Oxygen Electrode during High Temperature Steam Electrolysis. Energies, 2022, 15, 2726.	3.1	18
104	Nitrogen oxide reaction with six-atom silver clusters supported on LTA zeolite. Physical Chemistry Chemical Physics, 2009, 11, 6664.	2.8	17
105	High-Frequency EPR Analysis of MnO <sub>2</sub> -Doped [Bi <sub>0.5</sub> Na <sub>0.5</sub> ]TiO <sub>3</sub> -BaTiO <sub>3</sub> Piezoelectric Ceramics – Manganese Oxidation States and Materials â€~Hardening'. Ferroelectrics, 2012, 428, 116-121.	0.6	17
106	Support Effects on Hydrogen Desorption, Isotope Exchange, Chemical Reactivity, and Magnetism of Platinum Nanoclusters in KL Zeolite. Journal of Physical Chemistry C, 2013, 117, 22732-22745.	3.1	17
107	Observing different modes of mobility in lithium titanate spinel by nuclear magnetic resonance. RSC Advances, 2017, 7, 25276-25284.	3.6	17
108	Photoelectrochemical application of thinâ€film silicon tripleâ€junction solar cell in batteries. Physica Status Solidi (A) Applications and Materials Science, 2016, 213, 1926-1931.	1.8	16

#	Article	IF	CITATIONS
109	Electrochemical analysis and mixed potentials theory of ionic liquid based Metal–Air batteries with Al/Si alloy anodes. Electrochimica Acta, 2018, 276, 399-411.	5.2	16
110	Electron-Zeeman Resolved Electron Paramagnetic Resonance Spectroscopy. Journal of Magnetic Resonance, 2001, 152, 276-287.	2.1	15
111	DEFECT STRUCTURE IN "SOFT" ( <font>Gd</font> , <font>Fe</font> )-CODOPED PZT 52.5/47.5 PIEZOELECTRIC CERAMICS. Functional Materials Letters, 2008, 01, 7-11.	1.2	15
112	Mixed Ionic–Electronic Conducting Li4Ti5O12 as Anode Material for Lithium Ion Batteries with Enhanced Rate Capability – Impact of Oxygen Non-Stoichiometry and Aliovalent Mg2+-Doping Studied by Electron Paramagnetic Resonance. Zeitschrift Fur Physikalische Chemie, 2015, 229, 1439-1450.	2.8	15
113	Investigation of the corrosion behavior of highly As-doped crystalline Si in alkaline Si–air batteries. Electrochimica Acta, 2018, 265, 292-302.	5.2	15
114	Anisotropy of the mechanical properties of Li1·3Al0·3Ti1·7(PO4)3 solid electrolyte material. Journal of Power Sources, 2019, 437, 226940.	7.8	15
115	Investigation of the Li–Co antisite exchange in Fe-substituted LiCoPO4 cathode for high-voltage lithium ion batteries. Energy Storage Materials, 2019, 22, 138-146.	18.0	15
116	Control of oxygen-to-carbon ratio and fuel utilization with regard to solid oxide fuel cell systems with anode exhaust gas recirculation: A review. Journal of Power Sources, 2022, 524, 231077.	7.8	15
117	Secondary-Phase Formation in Spinel-Type LiMn2O4-Cathode Materials for Lithium-Ion Batteries: Quantifying Trace Amounts of Li2MnO3 by Electron Paramagnetic Resonance Spectroscopy. Applied Magnetic Resonance, 2018, 49, 415-427.	1.2	14
118	Impact of the charging conditions on the discharge performance of rechargeable iron-anodes for alkaline iron–air batteries. Journal of Applied Electrochemistry, 2018, 48, 451-462.	2.9	14
119	Flexible All-Solid-State Li-Ion Battery Manufacturable in Ambient Atmosphere. ACS Applied Materials & Interfaces, 2020, 12, 37067-37078.	8.0	14
120	Operando Transmission Electron Microscopy Study of All-Solid-State Battery Interface: Redistribution of Lithium among Interconnected Particles. ACS Applied Energy Materials, 2020, 3, 5101-5106.	5.1	14
121	ZnFe2O4 hollow rods enabling accelerated polysulfide conversion for advanced lithium-sulfur batteries. Electrochimica Acta, 2022, 414, 140231.	5.2	14
122	Single-Ion-Conducting "Polymer-in-Ceramic―Hybrid Electrolyte with an Intertwined NASICON-Type Nanofiber Skeleton. ACS Applied Materials & Interfaces, 2021, 13, 61067-61077.	8.0	14
123	SPACE-CHARGE LAYER, INTRINSIC "BULK" AND SURFACE COMPLEX DEFECTS IN <font>ZnO</font> NANOPARTICLES — A HIGH-FIELD ELECTRON PARAMAGNETIC RESONANCE ANALYSIS. Functional Materials Letters, 2013, 06, 1330004.	1.2	13
124	Erosion behavior of Y <sub>2</sub> O <sub>3</sub> in fluorineâ€based etching plasmas: Orientation dependency and reaction layer formation. Journal of the American Ceramic Society, 2021, 104, 1465-1474.	3.8	13
125	Integrated Coâ€Electrolysis and Syngas Methanation for the Direct Production of Synthetic Natural Gas from CO <sub>2</sub> and H <sub>2</sub> O. ChemSusChem, 2021, 14, 2295-2302.	6.8	13
126	Fabrication and interfacial characterization of Ni-rich thin-film cathodes for stable Li-ion batteries. Electrochimica Acta, 2021, 398, 139316.	5.2	13

#	Article	IF	CITATIONS
127	Characterization of the high-spin Mn 2 + -functional centre in BaTiO_3 by means of right-angle wiggling electron paramagnetic resonance spectroscopy. Molecular Physics, 2007, 105, 2195-2201.	1.7	12
128	Characterization of tetravalent vanadium functional centres in metal oxides derived from a spin-Hamiltonian analysis. Molecular Physics, 2012, 110, 277-282.	1.7	12
129	Electrode thickness-dependent formation of porous iron electrodes for secondary alkaline iron-air batteries. Electrochimica Acta, 2019, 314, 61-71.	5.2	12
130	Direct Solid Oxide Electrolysis of Carbon Dioxide: Analysis of Performance and Processes. Processes, 2020, 8, 1390.	2.8	12
131	Atomic-scale investigation of Na3V2(PO4)3 formation process in chemical infiltration via in situ transmission electron microscope for solid-state sodium batteries. Nano Energy, 2021, 87, 106144.	16.0	12
132	Instability of the Li <sub>7</sub> SiPS <sub>8</sub> Solid Electrolyte at the Lithium Metal Anode and Interphase Formation. Chemistry of Materials, 2022, 34, 3659-3669.	6.7	12
133	Right-angle wiggling electron paramagnetic resonance spectroscopy. Journal of Chemical Physics, 2001, 115, 9126-9135.	3.0	11
134	<font>Eu</font> <sup>2+</sup> -doped <font>CsBr</font> photostimulable X-ray storage phosphors — analysis of defect structure by high-frequency EPR. Functional Materials Letters, 2014, 07, 1350073.	1.2	11
135	Influence of PbO stoichiometry on the properties of PZT ceramics and multilayer actuators. Journal of the American Ceramic Society, 2019, 102, 5401-5414.	3.8	11
136	Analysis on discharge behavior and performance of As- and B-doped silicon anodes in non-aqueous Si–air batteries under pulsed discharge operation. Journal of Applied Electrochemistry, 2020, 50, 93-109.	2.9	11
137	Transient morphology of lithium anodes in batteries monitored by in operando pulse electron paramagnetic resonance. Communications Materials, 2021, 2, .	6.9	11
138	Formation of a Stable Solid-Electrolyte Interphase at Metallic Lithium Anodes Induced by LiNbO <sub>3</sub> Protective Layers. ACS Applied Energy Materials, 2021, 4, 10333-10343.	5.1	11
139	Structural Study of Polyacrylonitrile-Based Carbon Nanofibers for Understanding Gas Adsorption. ACS Applied Materials & Interfaces, 2021, 13, 46665-46670.	8.0	11
140	Quantifying local pH changes in carbonate electrolyte during copper-catalysed \$\$hbox {CO}_2\$\$ electroreduction using in operando \$\$^{13}hbox {C}\$\$ NMR. Scientific Reports, 2022, 12, 8274.	3.3	11
141	Analyzing the defect structure of CuO-Doped PZT and KNN piezoelectrics from electron paramagnetic resonance. IEEE Transactions on Ultrasonics, Ferroelectrics, and Frequency Control, 2014, 61, 1447-1455.	3.0	10
142	Dynamics of [Pyr <sub>13</sub> ][Tf <sub>2</sub> N] ionic liquid confined to carbon black. Physical Chemistry Chemical Physics, 2019, 21, 17018-17028.	2.8	10
143	On the reaction rate distribution in porous electrodes. Electrochemistry Communications, 2020, 121, 106865.	4.7	10
144	Signal Origin of Electrochemical Strain Microscopy and Link to Local Chemical Distribution in Solid State Electrolytes. Small Methods, 2021, 5, 2001279.	8.6	10

#	Article	IF	CITATIONS
145	Lithium deposition in single-ion conducting polymer electrolytes. Cell Reports Physical Science, 2021, 2, 100496.	5.6	10
146	Improved Electrochemical Performance of Zinc Anodes by EDTA in Nearâ€Neutral Zincâ''Air Batteries. Batteries and Supercaps, 2021, 4, 1830-1842.	4.7	10
147	Unraveling the State of Charge-Dependent Electronic and Ionic Structure–Property Relationships in NCM622 Cells by Multiscale Characterization. ACS Applied Energy Materials, 2022, 5, 1731-1742.	5.1	10
148	Li+ concentration waves in a liquid electrolyte of Li-ion batteries with porous graphite-based electrodes. Energy Storage Materials, 2022, 48, 475-486.	18.0	10
149	Exploring the Solvation Sphere and Spatial Accumulation of Dissolved Transition-Metal Ions in Batteries: A Case Study of Vanadyl Ions Released from V <sub>2</sub> O <sub>5</sub> Cathodes. ACS Applied Energy Materials, 2022, 5, 449-460.	5.1	9
150	Defects and Phase Formation in Non-Stoichiometric LaFeO <sub>3</sub> : a Combined Theoretical and Experimental Study. Chemistry of Materials, 2021, 33, 9473-9485.	6.7	9
151	An Advanced All Phosphate Lithium-Ion Battery Providing High Electrochemical Stability, High Rate Capability and Long-Term Cycling Performance. Journal of the Electrochemical Society, 2017, 164, A370-A379.	2.9	8
152	Coordination of the Mn <sup>4+</sup> -Center in Layered Li[Co <sub>0.98</sub> Mn <sub>0.02</sub> ]O <sub>2</sub> Cathode Materials for Lithium-Ion Batteries. Zeitschrift Fur Physikalische Chemie, 2017, 231, 905-922.	2.8	8
153	Co-Electrolysis, Quo Vadis?. ECS Transactions, 2017, 78, 3139-3147.	0.5	8
154	Physicochemical Mechanisms of the Double-Layer Capacitance Dispersion and Dynamics: An Impedance Analysis. Journal of Physical Chemistry C, 2021, 125, 5870-5879.	3.1	8
155	Complexions at the Electrolyte/Electrode Interface in Solid Oxide Cells. Advanced Materials Interfaces, 2021, 8, 2100967.	3.7	8
156	Fracture behavior of solid electrolyte LATP material based on micro-pillar splitting method. Journal of the European Ceramic Society, 2021, 41, 5240-5247.	5.7	8
157	Complexation of Copper(II)â^'Chelidamate:Â A Multifrequency-Pulsed Electron Paramagnetic Resonance and Electron Nuclear Double Resonance Analysis. Journal of Physical Chemistry B, 2006, 110, 20655-20663.	2.6	7
158	Transformation of carbon-supported Pt–Ni octahedral electrocatalysts into cubes: toward stable electrocatalysis. Nanoscale, 2018, 10, 21353-21362.	5.6	7
159	Sustainable Syngas Production by Highâ€Temperature Coâ€electrolysis. Chemie-Ingenieur-Technik, 2020, 92, 40-44.	0.8	7
160	Oxygen Nonstoichiometry and Valence State of Manganese in La <sub>1–<i>x</i></sub> Ca <sub><i>x</i></sub> MnO <sub>3+δ</sub> . ACS Omega, 2021, 6, 9638-9652.	3.5	7
161	An electrochemical cell for in operando <sup>13</sup> C nuclear magnetic resonance investigations of carbon dioxide/carbonate processes in aqueous solution. Magnetic Resonance, 2021, 2, 265-280.	1.9	7
162	Active Interphase Enables Stable Performance for an Allâ€Phosphateâ€Based Composite Cathode in an Allâ€Solidâ€State Battery. Small, 2022, 18, e2200266.	10.0	7

#	Article	IF	CITATIONS
163	CO <sub>2</sub> /N <sub>2</sub> Separation on Highly Selective Carbon Nanofibers Investigated by Dynamic Gas Adsorption. ChemSusChem, 2022, 15, .	6.8	7
164	Polarization-transfer electron-Zeeman resolved EPR. Chemical Physics Letters, 2002, 358, 271-277.	2.6	6
165	Characterization of non-stoichiometric co-sputtered Ba0.6Sr0.4(Ti1 â^' x Fe x )1 + x O3 â^' tunable passive microwave applications. Analytical and Bioanalytical Chemistry, 2012, 403, 643-650.	δthir 3.7	n films for
166	Insights into Water Interaction at the Interface of Nitrogen-Functionalized Hydrothermal Carbons. Journal of Physical Chemistry C, 2019, 123, 25146-25156.	3.1	6
167	Accessing Lithium–Oxygen Battery Discharge Products in Their Native Environments via Transmission Electron Microscopy Grid Electrode. ACS Applied Energy Materials, 2020, 3, 9509-9515.	5.1	6
168	Enhanced sulfur utilization in lithium-sulfur batteries by hybrid modified separators. Materials Today Communications, 2021, 26, 102133.	1.9	6
169	Analysis of the DRT as Evaluation Tool for EIS Data Analysis. ECS Transactions, 2021, 103, 1403-1412.	0.5	6
170	The role of the double layer for the pseudocapacitance of the hydrogen adsorption on platinum. Scientific Reports, 2022, 12, 3375.	3.3	6
171	Measurement of spin–lattice relaxation times in EPR with enhanced orientation selectivity. Journal of Magnetic Resonance, 2003, 162, 380-384.	2.1	5
172	Interplay between Defect Structure and Catalytic Activity in the Mo <sub>10â~'<i>x</i></sub> V <sub><i>x</i></sub> O <sub><i>y</i></sub> Mixedâ€Oxide System. ChemPhysChem, 2011, 12, 3578-3583.	2.1	5
173	The Impact of Heat Treatment on the Domain Configuration and Strain Behavior in Pb[Zr,Ti]O <sub>3</sub> Ferroelectrics. Journal of the American Ceramic Society, 2015, 98, 269-277.	3.8	5
174	Identification of LiPF 6 Decomposition Products in Liâ€lon Batteries with Endogenous Vanadyl Sensors Using Pulse Electron Paramagnetic Resonance and Density Functional Theory. Advanced Energy and Sustainability Research, 0, , 2100121.	5.8	5
175	Boundary Investigation of High-Temperature Co-Electrolysis Towards Direct CO <sub>2</sub> Electrolysis. Journal of the Electrochemical Society, 2022, 169, 034531.	2.9	5
176	Monitoring the reaction between lithium manganese spinel and Li2MnO3 during heat treatment using Electron Paramagnetic Resonance (EPR) spectroscopy. Solid State Ionics, 2018, 325, 201-208.	2.7	4
177	Post-Test Raman Investigation of Silver Based Gas Diffusion Electrodes. Journal of the Electrochemical Society, 2020, 167, 086505.	2.9	4
178	Polyethylene oxideâ€Li 6.5 La 3 Zr 1.5 Ta 0.5 O 12 hybrid electrolytes: Lithium salt concentration and biopolymer blending. Electrochemical Science Advances, 2021, 1, e2000029.	2.8	4
179	Study of CO <sub>2</sub> Sorption Kinetics on Electrospun Polyacrylonitrileâ€Based Carbon Nanofibers. Chemical Engineering and Technology, 2021, 44, 1168-1177.	1.5	4
180	Lithium intercalation into graphite: In operando analysis of Raman signal widths. Electrochemical Science Advances, 2022, 2, e2100068.	2.8	4

#	Article	IF	CITATIONS
181	Solvation and Ionâ€Pairing Effects of Choline Acetate Electrolyte in Protic and Aprotic Solvents Studied by NMR Titrations. ChemPhysChem, 2022, 23, .	2.1	4
182	Investigating the Interface between Ceramic Particles and Polymer Matrix in Hybrid Electrolytes by Electrochemical Strain Microscopy. Nanomaterials, 2022, 12, 654.	4.1	4
183	lon transport and limited currents in supporting electrolytes and ionic liquids. Scientific Reports, 2022, 12, 6215.	3.3	4
184	Coherence-transfer right-angle wiggling EPR. Molecular Physics, 2002, 100, 3661-3665.	1.7	3
185	Electron Paramagnetic Resonance Structure Investigation of Copper Complexation in a Hemicarcerand. Journal of Physical Chemistry B, 2006, 110, 15012-15020.	2.6	3
186	Hydrogen interstitial defects in acceptor-type CuO-doped PbTiO3—Uptake and dissolution of water vapor and formation of (CuTi″â~'(OH)O•)′ defect complexes. Applied Physics Letters, 2016, 109, 122904.	3.3	3
187	Warum wir uns mit Powerâ€ŧoâ€X beschÃŧtigen. Chemie-Ingenieur-Technik, 2020, 92, 3-3.	0.8	3
188	Ultrathin 2D Fe-Nanosheets Stabilized by 2D Mesoporous Silica: Synthesis and Application in Ammonia Synthesis. ACS Applied Materials & Interfaces, 2021, 13, 30187-30197.	8.0	3
189	A Dynamic Transmission Line Model to Describe the Potential Dependence of Double-Layer Capacitances in Cyclic Voltammetry. Journal of Physical Chemistry C, 0, , .	3.1	3
190	Tuning the moisture stability of multiphase βâ€Li <sub>3</sub> PS <sub>4</sub> solid electrolyte materials. Electrochemical Science Advances, 2023, 3, .	2.8	3
191	Ionic transport modeling for liquid electrolytes ―Experimental evaluation by concentration gradients and limited currents. Electrochemical Science Advances, 0, , .	2.8	3
192	Electron spin echo envelope modulation spectroscopy with g-value and orientation filters. Chemical Physics Letters, 2006, 417, 222-229.	2.6	2
193	Structural Characterization of Cu <sup>2+</sup> Functional Centers In â€~Lead-Free' KNN Piezoelectrics. Materials Research Society Symposia Proceedings, 2009, 1199, 7.	0.1	2
194	Influence of the A/B Stoichiometry on Defect Structure, Sintering, and Microstructure in Undoped and Cu-Doped KNN. , 2012, , 209-251.		2
195	Modeling 3D-Deposition of TiO2 Using a Monte Carlo Chemical Kinetics Approach. Journal of Physical Chemistry C, 2016, 120, 23823-23835.	3.1	2
196	Performance and Stability of Nickelates Based Oxygen Electrodes for Solid Oxide Cells. ECS Transactions, 2021, 103, 1505-1515.	0.5	2
197	Visualizing the Atomic Structure Between YSZ and LSM: An Interface Stabilized by Complexions?. ECS Transactions, 2021, 103, 1331-1337.	0.5	2
198	Modeling of Multi-Physics Phenomena for High-Temperature Co-Electrolysis. ECS Transactions, 2021, 103, 797-805.	0.5	2

#	Article	IF	CITATIONS
199	<i>Operando</i> transmission electron microscopy of battery cycling: thickness dependent breaking of TiO <sub>2</sub> coating on Si/SiO <sub>2</sub> nanoparticles. Chemical Communications, 2022, 58, 3130-3133.	4.1	2
200	LSC Infiltrated LSCF Oxygen Electrode for High Temperature Steam Electrolysis. ECS Transactions, 2017, 78, 3283-3295.	0.5	1
201	Thin Film Batteries: Origin of Degradation in Si-Based All-Solid-State Li-Ion Microbatteries (Adv. Energy) Tj ETQq1 1	0.78431	4 gBT /Ove
202	Investigation of La <sub>2-X</sub> Sr <sub>x</sub> Ni <sub>0.8</sub> Co <sub>0.2</sub> O <sub>4+d </sub> (0.0 ≤ ≤0.2) Materials as Oxygen Electrodes for Solid Oxide Cells. ECS Transactions, 2021, 103, 1517-1524.	0.5	1
203	Performance and Processes of Pure CO2 Electrolysis in Solid Oxide Cells. ECS Meeting Abstracts, 2021, MA2021-03, 216-216.	0.0	1
204	Performance and Processes of Pure CO <sub>2</sub> Electrolysis in Solid Oxide Cells. ECS Transactions, 2021, 103, 501-509.	0.5	1
205	Microstructural details of spindle-like lithium titanium phosphate revealed in three dimensions. RSC Advances, 2021, 11, 34605-34612.	3.6	1
206	Independent component analysis combined with Laplace inversion of spectrally resolved spin-alignment echo/ <i>T</i> <sub>1</sub> 3D <sup>7</sup> Li NMR of superionic Li <sub>10</sub> GeP <sub>2</sub> S <sub>12</sub> . Zeitschrift Fur Physikalische Chemie, 2022, 236, 899-922.	2.8	1
207	Sr Substituted La2â~'xSrxNi0.8Co0.2O4+δ (0 ≤ ≤0.8): Impact on Oxygen Stoichiometry and Electrochemical Properties. Energies, 2022, 15, 2136.	3.1	1
208	Soft-sensor based operation of a solid oxide fuel cell system with anode exhaust gas recirculation. Journal of Power Sources, 2022, 532, 231354.	7.8	1
209	Feasibility and Limitations of High-Voltage Lithium-Iron-Manganese Spinels. Journal of the Electrochemical Society, 2022, 169, 070518.	2.9	1
210	Characterization of the defect structure in acceptor- and donor-doped PZT ceramics. Applications of Ferroelectrics, IEEE International Symposium on, 2007, , .	0.0	0
211	Heat treatment effects on domain configuration and strain under electric field in undoped Pb[Zr <inf>x</inf> Ti <inf>1−x</inf> ]O <inf>3</inf> ferroelectrics. , 2013, , .		0
212	Modeling of Multi-Physics Phenomena for High-Temperature Co-Electrolysis. ECS Meeting Abstracts, 2021, MA2021-03, 148-148.	0.0	0
213	Investigation of La2-XSrxNi0.8Co0.2O4+d (0.0 ≤ ≤0.2) Materials as Oxygen Electrodes for Solid Oxide Cells. ECS Meeting Abstracts, 2021, MA2021-03, 139-139.	0.0	0
214	Visualizing the Atomic Structure Between YSZ and LSM: An Interface Stabilized by Complexions?. ECS Meeting Abstracts, 2021, MA2021-03, 52-52.	0.0	0
215	Understanding High-Temperature Electrolysis. ECS Meeting Abstracts, 2021, MA2021-03, 214-214.	0.0	0
216	Boundaries of High-Temperature Co-Electrolysis Towards Direct CO2-Electrolysis. ECS Transactions, 2021, 103, 493-500.	0.5	0

#	Article	IF	CITATIONS
217	Analysis of the DRT as Evaluation Tool for EIS Data Analysis. ECS Meeting Abstracts, 2021, MA2021-03, 61-61.	0.0	0
218	Boundaries of High-Temperature Co-Electrolysis Towards Direct CO2-Electrolysis. ECS Meeting Abstracts, 2021, MA2021-03, 215-215.	0.0	0
219	Performance and Stability of Nickelates Based Oxygen Electrodes for Solid Oxide Cells. ECS Meeting Abstracts, 2021, MA2021-03, 137-137.	0.0	0
220	Understanding High-Temperature Electrolysis. ECS Transactions, 2021, 103, 487-492.	0.5	0
221	Online characterization of operational parameters in an SOFC system with anodeâ€exhaust gas recirculation by oxygen sensors. Fuel Cells, 0, , .	2.4	0
222	The effect of cobalt on morphology, structure, and ORR activity of electrospun carbon fibre mats in aqueous alkaline environments. Beilstein Journal of Nanotechnology, 2021, 12, 1173-1186.	2.8	0
223	Inâ€situ hydrogen evolution monitoring during the electrochemical formation and cycling of pressedâ€plate carbonyl iron electrodes in alkaline electrolyte. Batteries and Supercaps, 0, , .	4.7	0
224	In Situ Hydrogen Evolution Monitoring During the Electrochemical Formation and Cycling of Pressedâ€Plate Carbonyl Iron Electrodes in Alkaline Electrolyte. Batteries and Supercaps, 0, , .	4.7	0